Indian Ocean Feedback to the ENSO Transition in a Multimodel Ensemble

JONG-SEONG KUG

Korea Institute of Ocean Science and Technology, Ansan, South Korea

YOO-GEUN HAM

Global Modeling and Assimilation Office, NASA GSFC, Greenbelt, and Goddard Earth Sciences Technology and Research Studies and Investigations, Universities Space Research Association, Columbia, Maryland

(Manuscript received 24 January 2012, in final form 20 April 2012)

ABSTRACT

Observational studies hypothesized that Indian Ocean (IO) feedback plays a role in leading to a fast transition of El Niño. When El Niño accompanies IO warming, IO warming induces the equatorial easterlies over the western Pacific (WP), leading to a rapid termination of El Niño via an oceanic adjust process. In this study, this IO feedback is reinvestigated using the Coupled Model Intercomparison Project phase 3 (CMIP3) coupled GCM simulations. It is found that most of the climate models mimic this IO feedback reasonably, supporting the observational hypothesis. However, most climate models tend to underestimate the strength of the IO feedback, which means the phase transition of ENSO due to the IO feedback is less effective than the observed one. Furthermore, there is great intermodel diversity in simulating the strength of the IO feedback. It is shown that the strength of the IO feedback is related to the precipitation responses to El Niño and IO SST forcings over the warm-pool regions. Moreover, the authors suggest that the distribution of climatological precipitation is one important component in controlling the strength of the IO feedback.

1. Introduction

In the tropics, climate variabilities over three Ocean basins (Pacific, Indian, and Atlantic Oceans) are tightly coupled, so interbasin interaction is quite important when determining the climate mean state and variability (Watanabe 2008a,b). In particular, many studies have reported the covariability and interaction between the El Niño–Southern Oscillation (ENSO) and the Indian Ocean (IO) sea surface Temperature (SST) (Klein et al. 1999; Venzke et al. 2000; Baquero-Bernal et al. 2002; Huang and Kinter 2002; Xie et al. 2002; Lau and Nath 2000, 2003, 2004; Krishnamurty and Kirtman 2003; Wu and Kirtman 2004; Kug et al. 2005). To a large extent, they all agreed that the modulation of the Walker circulation via atmospheric teleconnection is a key mechanism linking the ENSO and IO variability.

While many previous studies have focused on the impact of ENSO on IO variability, the role of the Indian Ocean in modulating ENSO characteristics has recently been highlighted by several researchers (Yu et al. 2002; Yu 2005; Saji and Yamagata 2003; Kug et al. 2005; Kug and Kang 2006; Watanabe and Jin 2002; 2003; Sooraj et al. 2009; Wu and Kirtman 2004; Annamalai et al. 2005, 2010; Ohba and Ueda 2007, 2009, Ohba et al. 2010; Yamanaka et al. 2009; Luo et al. 2010; Izumo et al. 2010). Among them, Kug and Kang (2006) emphasized the Indian Ocean feedback to the ENSO transition. They pointed out that IO warming tends to be accompanied by El Niño during the El Niño developing phase, then the IO warming leads to a rapid decay of the El Niño event and a fast transition to La Niña.

The dynamical process of interaction between ENSO and IO variability is as follows. During the developing phase of El Niño, the tropical Pacific forcing tends to induce equatorial easterlies over the eastern IO, which leads to the western IO warming. The equatorial easterlies and warming over IO can be enhanced by the local air–sea interaction (Webster et al. 1999; Saji et al. 1999; Li et al. 2002). During El Niño's mature phase, IO warming affects the Pacific variability. That is, IO warming modulates anomalous Walker circulation and generates anomalous equatorial easterlies over the western Pacific (WP) with enhanced anticyclonic circulation over the western

Corresponding author address: Dr. Yoo-Geun Ham, NASA Goddard Space Flight Center, Code 610.1, Greenbelt, MD 20771. E-mail: yoo-geun.ham@nasa.gov

DOI: 10.1175/JCLI-D-12-00078.1

© 2012 American Meteorological Society

North Pacific. The WP easterlies play a role in shoaling equatorial thermocline via Kelvin wave adjustment, which plays a role in the rapid decay of the eastern Pacific SST. During the subsequent spring and summer, IO warming persists and continuously affects the WP easterly wind even after the eastern Pacific SST has vanished (Xie et al. 2009). Therefore, the IO feedback plays a role in enhancing the phase transition from El Niño to La Niña.

Because of the limited length of historical observational data, several studies tried to examine this process in current climate models (Kug et al. 2006a,b; Ohba and Ueda 2007; Ohba and Watanabe 2012), and revealed that the IO feedback to ENSO transition still works to some extent in these climate models. However, current state-of-the-art climate models still have difficulty simulating IO variability (Saji et al. 2006). In particular, there is great diversity in simulating the covariability between ENSO and IO variability, which indicates that the strength of IO feedback can differ among climate models. Because IO variability is a critical component of ENSO prediction (Luo et al. 2010; Izumo et al. 2010), it is important to understand why climate models simulate IO feedback so differently. Furthermore, the model diversity can provide a critical information for simulating IO feedback to the ENSO that could serve as a guide for future model improvement.

In this study, we examine model fidelity in simulating IO feedback in the CMIP3 multimodel framework. Our objectives are (i) to test the observational hypothesis regarding IO feedback into the ENSO transition using multimodel frameworks, and (ii) to examine model diversity in simulating IO feedback and determine what causes the diversity and systematic biases in the current models.

Section 2 gives a brief description of the observational data and model simulation. In section 3, we examine the IO feedback in the CMIP3 climate models. Section 4 discusses model diversity in simulating IO feedback. A summary and discussion are provided in section 5.

2. Data

To examine IO feedback in current climate models, we analyze 18 climate models using the preindustrial (''picntrl'') runs from the Couple Model Intercomparison phase 3 (CMIP3) archives. The CO_2 concentration of the preindustrial run is fixed at 280 ppm for the whole integration period. Model references, details on the institutions where the models were run, and integration periods are summarized in Table 1.

To verify the model output, we use observed monthly-mean atmospheric and oceanic data. The observed SST data are the improved Extended Reconstructed Sea Surface Temperature (SST) version 3 (ERSST V.3; Smith et al. 2008) from the United States National Climatic Data Center. This data uses 1° spatial resolution super-observations, which are defined as individual observations averaged into a 1° bin. The monthly-mean winds are from the National Centers for Environmental Prediction (NCEP)–National Center for Atmospheric Research (NCAR) reanalysis (Kalnay et al. 1996). They have a horizontal resolution of 2.5° × 2.5°. The period of SST and winds is 52 years from 1958 to 2009 during December–February (DJF).

3. Role of IO feedback in climate models

To examine IO feedback in climate models, we first define El Niño events as those occurring when the Niño 3.4 SST anomaly (area-averaged SST anomalies over 5°S–5°N, 170°–120°W) during December to the following February (i.e., DJF season) is greater than its standard deviation in each model. Because we use long-term climate simulation (several hundred years; Table 1) we can include more cases for the composite analyses than the observed. Next, we separate the El Niño events into two groups depending on the IO SST index, which is defined as the area-averaged SST anomalies over the Indian Ocean (15°S–10°N, 40°–110°E) during the DJF season. Note that the region representing IO warming is similar to that in Yu and Lau (2005). One group is El Niño accompanied by IO warming (i.e., the IO SST index is greater than its standard deviation), and the other is El Niño only, which does not accompany IO warming (i.e., the IO SST index is less than one standard deviation). Since the standard deviation is calculated from each model simulation, the degree of IO warming differs among the climate models.

Figure 1 shows the evolution of Niño-3.4 SST for IO warming and El Nino only cases. It is evident from the figure that there is a distinctive evolution of SST between the two. In the case of IO warming, the positive Niño-3.4 SST rapidly decays and La Niña develops in the subsequent winter. Since the major time scale of ENSO is known to be about four years, it is clear that such a transition is relatively fast. The IO SST tends to slowly develop during El Niño developing and mature phase, and its magnitude is at maximum during March–May (MAM) of the decaying phase, indicating a delayed response (Klein et al. 1999). Therefore, the IO warming can play a role in modulating ENSO phase transition. In contrast, when IO warming is not accompanied (El Niño only case), the decay of the Niño-3.4 SST is relatively slow, reaching a normal state during the subsequent winter season. This suggests that IO warming plays some

TABLE 1. Descriptions of models in the CMIP3 archives.

Modeling group	Model number in this study	CMIP ID (label in figures)	AGCM resolution (horizontal, vertical)	OGCM resolution (horizontal, vertical)	Integration period
National Oceanic and Atmospheric Administration/ Geophysical Fluid Dynamics Laboratory NOAA/GFDL	3	GFDL CM2.1	2.5 × 2.0 L24	1 × 0.33 at equator L50	500 yr
Istituto Nazionale di Geofisica e Vulcanologia (Italy) (INGV)	4	INGV ECHAM4	1.125 × 1.125 L19	2 × 1 at equator L33	100 yr
Commonwealth Scientific and Industrial Research Organisation (CSIRO) Atmospheric Research	5	CSIRO Mk3.0	T63 L18	1.875 × 0.84 L31	380 yr
	6	CSIRO Mk3.5	T63 L18	1.875 × 0.84 L31	500 yr
Center for Climate Research Studies (CCSR), Japan Marine Science and Technology Center (JAMSTEC)	7	Model for Interdisciplinary Research on Climate 3.2, medium-resolution version [MIROC3.2(medres)]	T42 L20	1.4 × 0.5 at equator L43	500 yr
Hadley Centre Met Office	8	Met Office (UKMO) Hadley Centre Global Environmental Model version 1 HadGEM1)	N96 L38	1 × 0.33 L40	240 yar
Bjerknes Center for Climate Research (BCCR)	9	BCCR model, version 2.0 (BCM2.0)	T63 L31	1.5 × 0.5 at equator L35	250 yr
NOAA/GFDL	10	GFDL Climate Model version 2.0 (GFDL CM2.0)	2.5 × 2.0 L24	1 × 0.33 at equator L50	500 yr
CCCma	11	CCCma CGCM3.1t63	T63 L32	1.4 × 0.94 L29	400 yar
L'Institut Pierre-Simon Laplace (IPSL)	12	IPSL Coupled Model, version 4 (IPSL CM4)	2.5 × 3.75 L19	2 × 2 L31	500 yr
Hadley Centre/Met Office	13	UKMO third climate configuration of the Met Office Unified Model (HadCM3)	3.75 × 2.75 L20	1.25 × 1.25 L20	340 yr
CCSR, JAMSTEC	14	MIROC3.2 high-resolution version [MIROC3.2(hires)]	T106 L56	T106 L48	100 yr
State Key Laboratory of Numerical Modeling for Atmospheric Sciences and Geophysical Fluid Dynamics (LASG)	15	Institute of Atmospheric hysics (IAP) Flexible Global Ocean–Atmosphere–Land System Model gridpoint version 1.0 (FGOALS-g1.0)	2.8 × 2.8 L26	1 × 1 L33	350 yrr
University of Bonn, Korea Meteorological Administration (KMA)	16	Meteorological Institute of the University of Bonn, ECHO-G Model (MIUBECHOG)	T30 L19	2.8125 × 0.5 at equator L20	340 yr
Institute of Numerical Mathematics (INM)	17	INM- Coupled Model, version 3.0 (CM3.0)	4 × 5 L21	2 × 2.5 L33	330 yr
Météo-France	18	Centre National de Recherches Météorologiques Coupled Global Climate Model, version 3 (CNRM-CM3)	T42 L45	2 × 0.5 at equator L31	500 yr
Meteorological Research Institute (MRI)	19	MRI Coupled General Circulation Model, version 2.3.2a (MRI CGCM2.3.2a)	T42 L30	2 × 0.5 at equator L23	350 yr
Canadian Centre for Climate Modelling and Analysis (CCCMA)	20	CCCma coupled GCM version 3.1 (CCma_CGCM3.1)	T47 L31	1.85 × 1.85 L29	500 yr

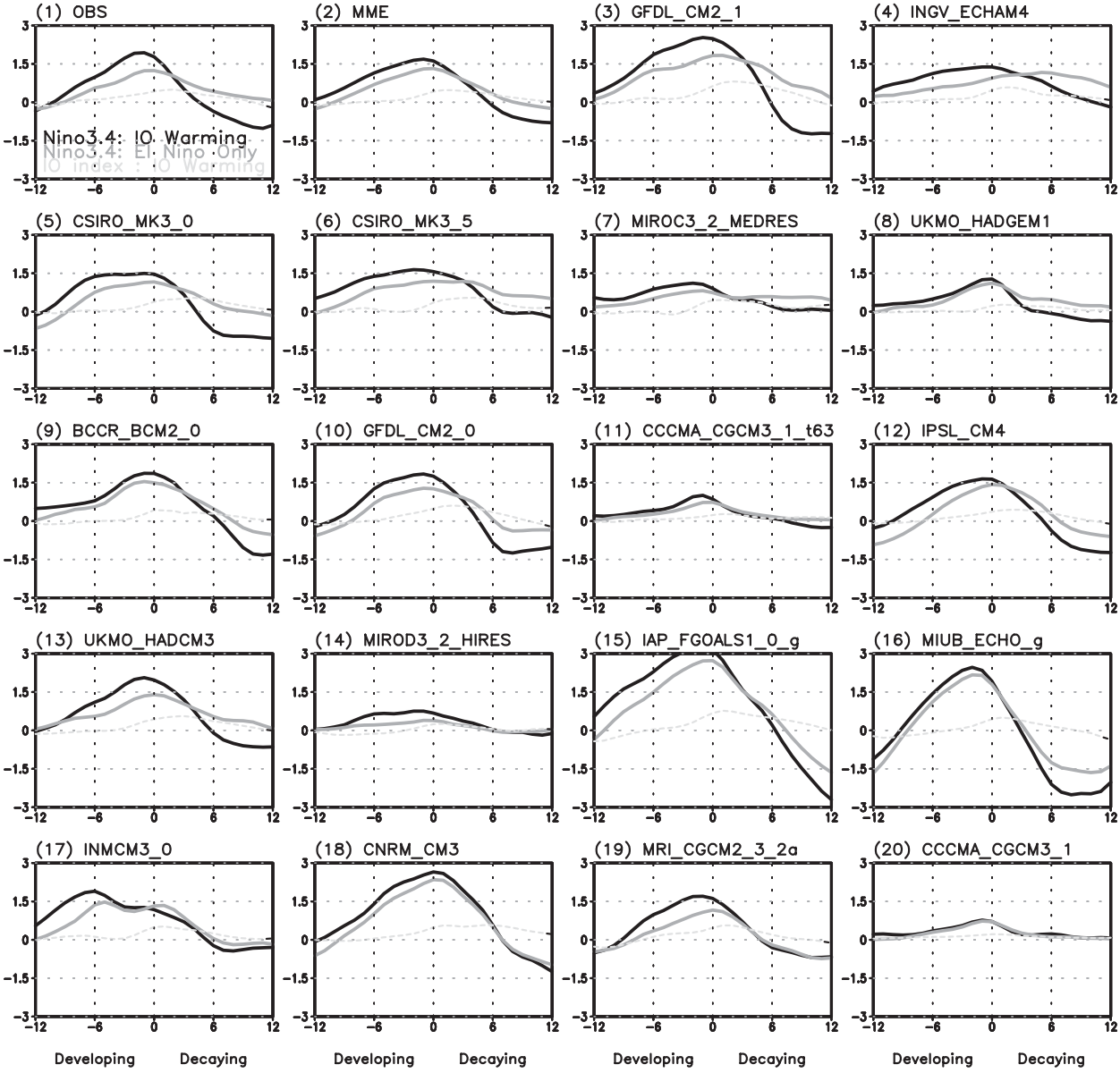

FIG. 1. The evolution of Niño-3.4 SST between the IO warming case (black line) and the El Niño only case (gray line) based on 1) observational data, the 2) multimodel ensemble (MME), and 3)–20) each climate model. The IO SST in IO warming case is also shown in gray dotted line. The numbers on the *x* axis denote the lag-month from the El Niño (or IO warming) peak during the DJF season. The Niño-3.4 SST is given in °C.

role in the fast transition of El Niño. These results are consistent with the findings of Kug and Kang (2006).

To a large extent, the current climate models tend to simulate IO feedback reasonably. Most of the 18 models simulate a faster transition from El Niño to La Niña in the presence of IO warming. The multimodel ensemble (MME) clearly shows that IO warming results in a rapid termination of El Niño and early development of La Niña, compared to El Niño without IO warming (Fig. 1b). However, it is also shown that a few models simulate almost similar evolution between two cases, indicating weak Indian Ocean feedback. It is noted that at least no model exhibits significantly slower transition for the IO warming case compared to the El Niño only case.

To measure degree of the fast transition, Fig. 2 shows the difference in Niño-3.4 SST one year after the El Niño mature phase (DJF) between the IO warming and El Niño only cases. To consider the different ENSO magnitudes among climate models, this difference is normalized by the standard deviation of Niño-3.4 SST in

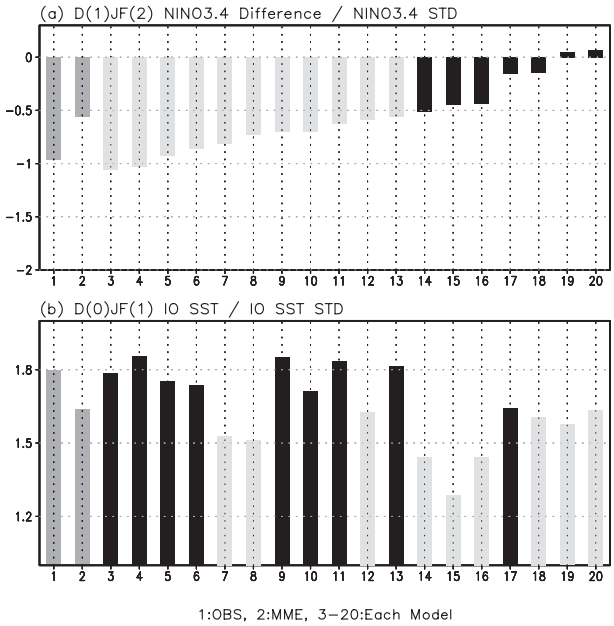

FIG. 2. (a) The difference in Niño-3.4 during the D(1)JF(2) season in the IO warming case compared to that in the El Niño only case. The difference in Niño-3.4 is divided by the standard deviation of Niño-3.4 in each model in order to consider the different ENSO magnitudes among the climate models. (b) The IO SST during the D(0)JF(1) season in the IO warming case divided by the standard deviation of IO SST in each model. Numbers 1, 2, and 3–20 denote the observational data, MME, and each climate model, respectively.

each model. Significant negative differences in Niño-3.4 SST are noted in both the observation and MME, indicating that the IO warming case is more likely to develop the La Niña phase one year after the El Niño mature phase. It is interesting that the MME seems to underestimate the IO feedback compared to the observed. While the observation shows about one standard deviation difference, the MME shows only a 0.56 standard deviation difference. In fact, the differences in most of the models are smaller than that in the observation. This indicates that the climate models simulate the IO feedback reasonably well, but they are still underestimating the strength of the IO feedback.

Another interesting point is that there is great diversity in the simulation of IO feedback among the CMIP3 climate models. Negative Niño-3.4 differences are simulated by 16 of the 18 models, implying robustness of the observed IO feedback. However, the differences vary from −1.05 to 0.06 standard deviations. In particular, the last four models exhibit distinctively weak negative or even positive differences, indicating weak IO feedback. As well as the strength of the IO feedback, climate models simulate quite different IO responses (Fig. 2b). The degree of the IO warming is spread between 0.2 to 0.8 K, though they are from the composites when the IO warming is greater than one standard deviation. At glance, the strength of the IO feedback is related to the degree of the IO warming. The correlation coefficient between them is 0.53, indicating that strong IO SST response lead to strong IO feedback. However, it is also found that some models have quite weak IO feedback in spite of a sizeable IO warming. In the next section we will discuss what control the strength of the IO feedback in climate models.

From Figs. 1 and 2, it is evident that there are distinctive differences in the phase transition between the two groups. However, the El Niño magnitude of the IO warming group tends to be greater than that of the El Niño only group. This is because strong El Niño events tend to accompany IO warming (Sooraj et al. 2009). Therefore, one may argue that the differences in phase transition are due to the different El Niño magnitudes, not IO warming. In fact, a strong El Niño tends to undergo a faster transition to La Niña than a moderate El Niño (An et al. 2005) due to strong zonal contrast in the equatorial thermocline, which leads to a strong discharge to off-equatorial regions (Jin 1997a,b). Therefore, we need to clarify whether the faster transition of ENSO in the IO warming group is due to IO warming or to strong El Niño magnitude.

To control for the dependence on El Niño magnitude, we conduct a conditional composite analysis by excluding strong El Niño events. For the conditional composites, we select El Niño events only when the Niño-3.4 SST is between one and two standard deviations. Therefore, as shown in Fig. 3, the magnitude of Niño-3.4 becomes almost similar between the two groups during the mature phase, though a few models still exhibit a higher Niño-3.4 SST in the case of IO warming. Though the difference in the evolution of Niño-3.4 SST is slightly reduced, the climate model still simulates a faster transition from El Niño to La Niña for the IO warming case compared to the El Niño only case, supporting the fact that IO warming is a critical component in the fast phase transition of ENSO.

How does IO warming lead to the fast transition of ENSO? As mentioned in the introduction, Kug and Kang (2006) hypothesized a possible dynamic process using the observational data. In this section, we will reexamine this dynamic process using the multimodel dataset. We perform a composite analyses of atmospheric and oceanic variables for both cases from the September–November (SON) [i.e., SON(0)] season before the El Niño peak season to the December–February [i.e., D(1)JF(2)] season the following year. Based on the composites from each model, we calculate multimodel ensemble results by simply averaging the composites.

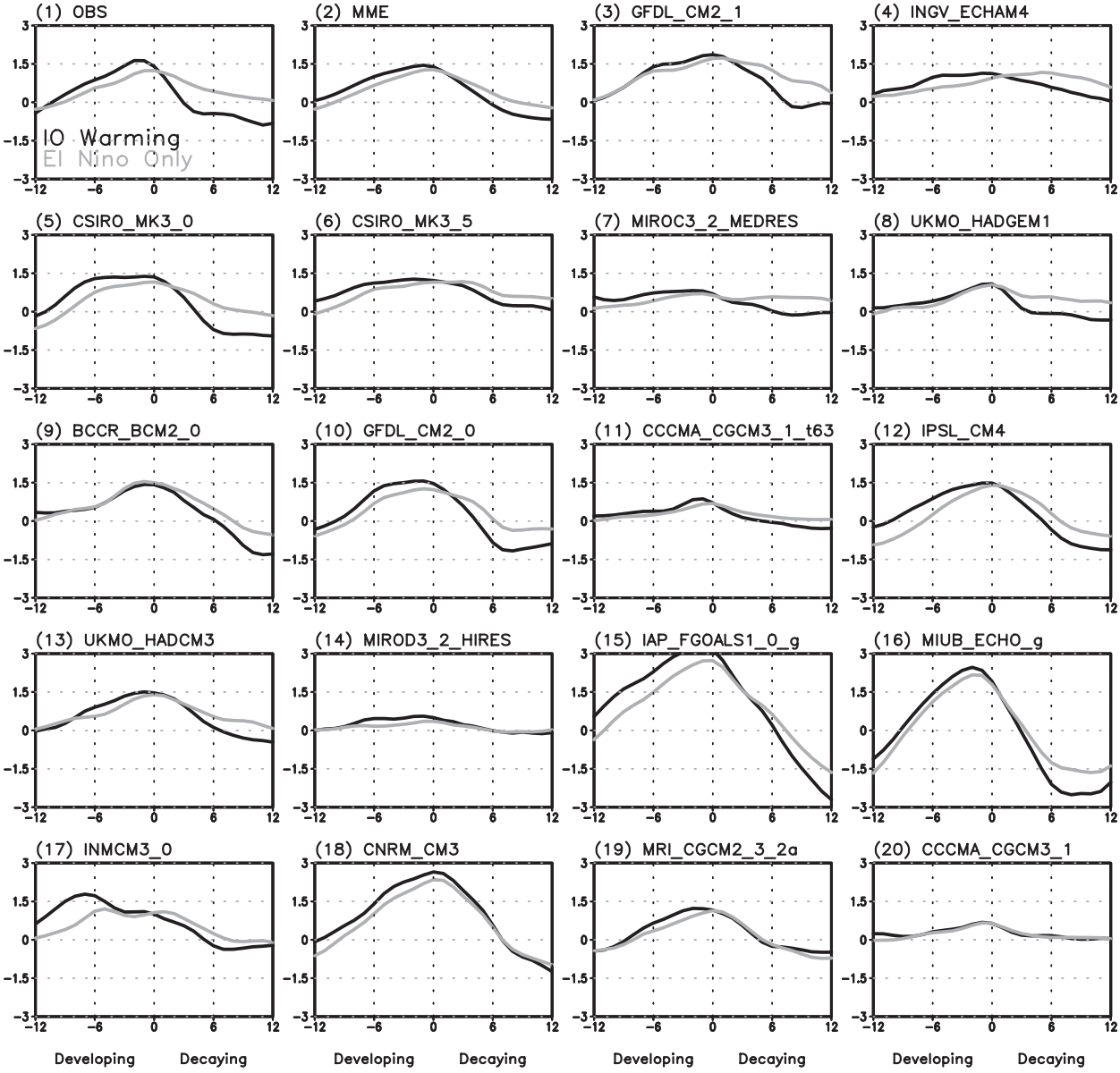

FIG. 3. As in Fig. 1, but the criteria for defining El Niño is much more confined in that the magnitude of Niño-3.4 is between one and two standard deviations.

Figure 4 shows SST composites for both cases. During the boreal autumn season, a positive SST develops over the equatorial Pacific in both cases. These positive SST anomalies extend too far to the western Pacific, which is a common problem with the state-of-art coupled GCMs (Wittenberg et al. 2006). As expected from Fig. 1, these SST anomalies are greater in the IO warming case. The positive SST anomalies over the western IO and negative SST anomalies over the eastern IO during SON(0) season are distinctive in the IO warming case, showing a dipole pattern (Saji et al. 1999). This dipole pattern evolves to the basinwide warming during boreal winter (Kug and Kang 2006; Izumo et al. 2010). It is interesting that the positive SST anomalies over the western IO are more distinctive than the negative anomalies over the eastern IO during boreal autumn, which is consistent with the observed one (Kug and Kang 2006), while the magnitude of SST anomalies over the eastern IO is usually greater than that over the western IO in the conventional IO dipole events (Saji et al. 1999). Some models exhibit the dipole pattern, but the others show only western IO warming, such that MME shows the stronger signal over the western Indian Ocean. This implies that western IO warming is more critical to basinwide

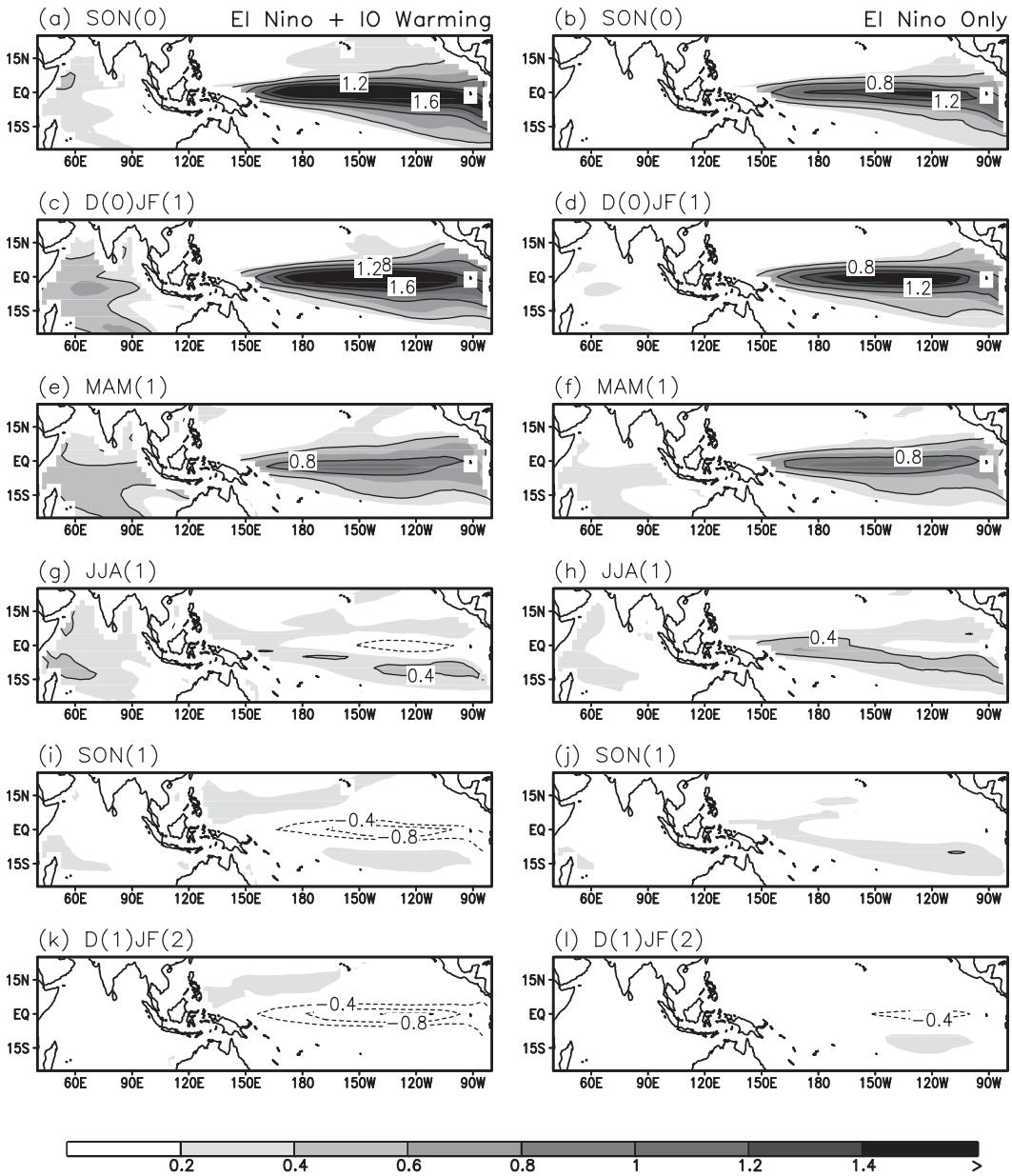

FIG. 4. Composite of MME SST anomalies (°C) for (left) the IO warming case and (right) the El Niño only case from the autumn season during the El Niño developing phase [SON(0)] to the winter season of the subsequent year [D(1)JF(2)].

warming in the following season and to the fast transition of ENSO.

The basinwide warming signal over the IO persists up to the following June–August [(JJA); JJA(1)] season in the case of IO warming when the eastern Pacific warming has mostly terminated. The persistent IO warming plays a role in altering atmospheric circulation as the so-called, ''capacitor effect'' (Yang et al. 2007; Li et al. 2007; Wu et al. 2009; Xie et al. 2009; Wu et al. 2010). During the JJA (1) season when the equatorial Pacific SST anomalies are nearly zero and negative SST anomalies occur in the case of the IO warming (Fig. 4g), there are still positive SST anomalies over the central Pacific for El Niño only (Fig. 4h). Once the negative SST anomalies are established over the eastern Pacific, they further develop into La Niña events until the following winter via strong Bjerknes feedback (Fig. 4k).

Figure 5 shows the precipitation composites, which are consistent with the SST composites. During the SON(0) season, there are positive precipitation anomalies over

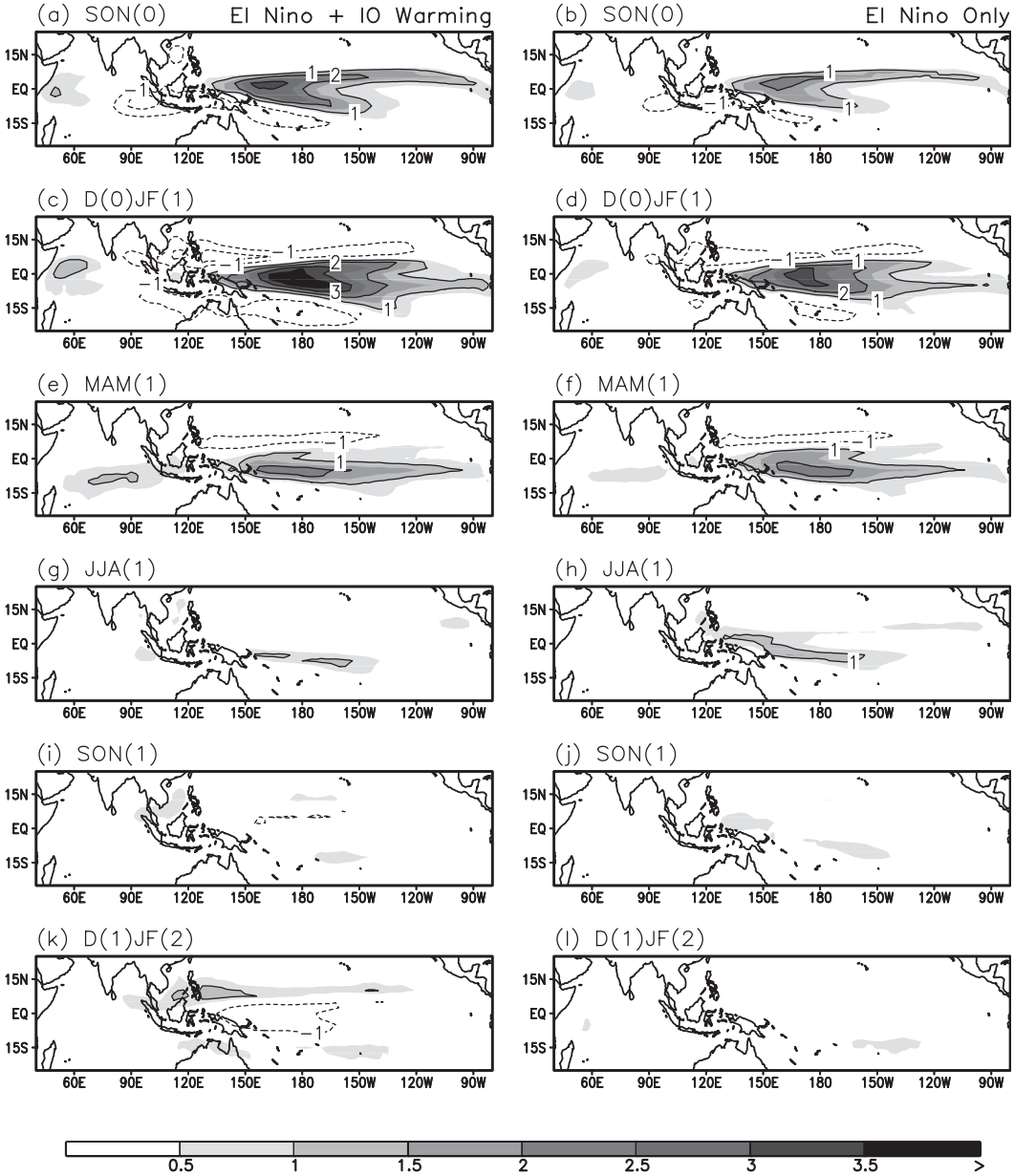

FIG. 5. As in Fig. 4, but MME precipitation anomalies (mm day^{-1}).

the western IO, which are related to the local positive SST anomalies. In addition, strong negative anomalies appear over the eastern IO, which are distinctive in spite of the weak SST anomalies. This indicates these negative precipitation anomalies might be caused remotely by strong upward motion over the tropical central Pacific and western Indian Ocean, and the remote forcing is important for inducing precipitation anomalies over the eastern IO during El Niño events. The distinctive dipole pattern of precipitation would induce equatorial easterlies, which in turn enhance the dipole SST pattern over IO.

During the boreal winter [D(0)JF(1) season, Fig. 5c], the negative precipitation anomalies weaken over the eastern IO, and the positive anomalies over the western IO intensify and expand. Instead, negative precipitation anomalies suddenly develop over the western North Pacific (WNP). Note that these negative precipitation anomalies are considerably stronger in the IO warming case than those in the El Niño only case. This difference might be due to the intensified positive precipitation anomalies over the western IO. Watanabe and Jin (2002, 2003) showed using the linear baroclinic model that the

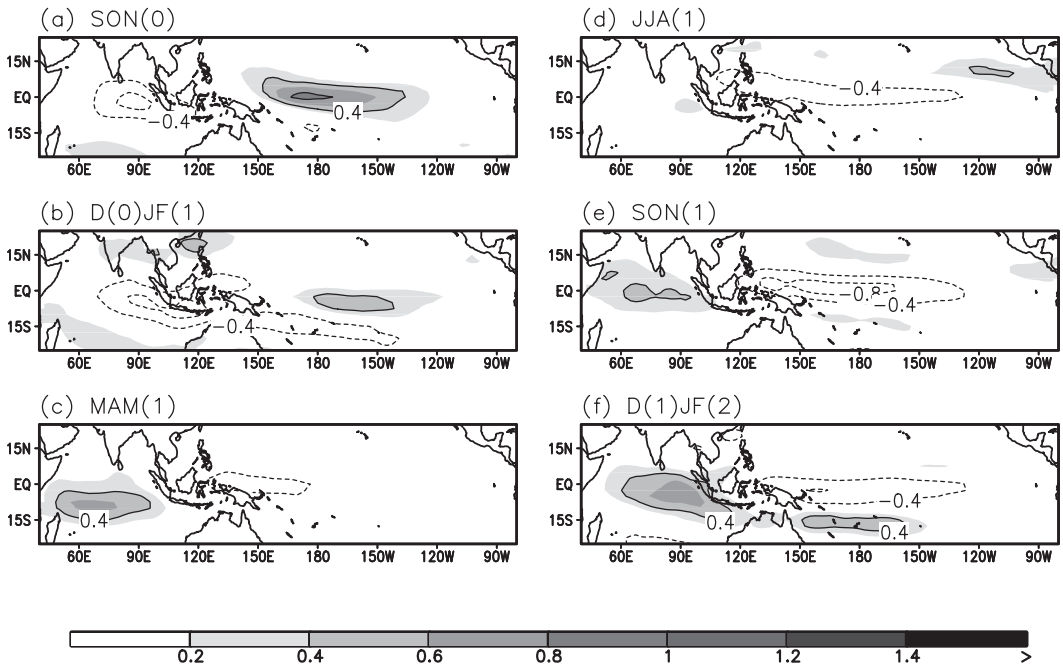

FIG. 6. The MME difference in zonal wind at 925 hPa (m s^{-1}) in the IO warming case compared to that in the El Niño only case.

positive precipitation anomalies modulate the Walker circulation, then induce anomalous sinking motion over the western North Pacific. The anomalous sinking motion induces anomalous precipitation response where the climatological convective activity is strong. The precipitation response lead to stronger sinking motion in turn, so the anomalies are intensified over the western North Pacific. Some AGCM and CGCM experiments support the role of the Indian Ocean SST in altering convective activity over the western North Pacific (Kug and Kang 2006; Kug et al. 2006b; Ohba and Ueda 2007).

This suppressed convection over the WNP leads to anomalous anticyclonic flow (Wang et al. 2000), which is linked to the equatorial easterly anomalies up to the following spring season [i.e., MAM(1) season]. The positive precipitation anomalies over the western IO in the D(0)JF(1) season, which intensify and expand in a previous season, persist up to the following spring while gradually shifting toward the eastern IO (Fig. 5e). Though the magnitude is quite weak, there are still positive precipitation anomalies over the eastern IO until boreal summer in the case of IO warming (Fig. 5g).

The precipitation difference leads to different wind responses. To clearly show the different wind evolution, Fig. 6 illustrates the difference in zonal wind at 925 hPa between the IO warming and the El Niño only cases. During the boreal autumn [SON(0)] season, it is clear that there are stronger westerly anomalies over the central Pacific and stronger easterly anomalies over the IO in the presence of IO warming. The stronger westerlies and easterlies in the IO warming case are related to stronger SST anomalies over the tropical Pacific, as shown in Figs. 4a and 4b. It is conceivable that the stronger easterlies over the IO are responsible for the significant dipole pattern of the SST as shown Fig. 4a. Note that this easterly difference is only confined to the IO during the SON(0) season, implying that the effect of the IO on the tropical Pacific is limited. However, during boreal winter the easterlies difference shifts to the east and expands to the western Pacific (Fig. 6b). Since there are also differences in the westerlies over 10°–20°N, indicating the zonally elongated anticyclones are strengthened in the case of IO warming. Note that the westerly difference over the central Pacific is weakened during boreal winter, but the easterly difference over the IO and western Pacific is intensified. This implies that such the easterly difference is due to both the IO SST and the Pacific SST.

During the MAM(1) season, the easterly difference is further shifted to the east and expanded to the western Pacific (Fig. 6c), and there is a westerly difference over the IO, which is consistent with the eastward movement of the IO precipitation anomalies as shown in Figs. 5c and 5e. The western Pacific easterlies enhance shoaling of the equatorial Pacific basin thermocline, which leads to fast termination of El Niño and the development of surface cooling over the eastern Pacific. Once surface cooling takes place, anomalous easterlies further develop

over the central Pacific, which is consistent with the development of La Niña (Figs. 6d-f).

The different evolution of low-level zonal wind is a critical component in determining the different phase transitions of ENSO. The differences in SST and zonal wind between the IO warming and El Niño warming cases shown in Figs. 4 and Fig. 6, respectively, can be caused by stronger warming of either the Pacific or IO. To standardize the different strengths of Pacific warming and emphasize the impact of differences in IO warming between the two cases, Fig. 7 shows the MME of equatorial zonal wind anomalies normalized by dividing Niño-3.4 SST from each composite. For this, we first calculate the normalized zonal wind anomalies in the IO warming and El Niño only cases by dividing the Niño-3.4 SST calculated from each case for each model, then the MME is calculated. Note that we simply assume that the wind response to Pacific warming is linear in spite of the fact that some nonlinearity exists. During the D(0)JF(1) season, the two composites have similar values to the east of the date line, which means that the magnitude of the westerly anomalies in this region is directly related to the Niño-3.4 SST. It also supports our linear assumption in this region. In contrast to the similar westerly anomalies over the central-eastern Pacific, there is a significant easterly difference over the eastern IO and western Pacific in the IO warming case. It can therefore be inferred that IO warming contributes to the easterly difference over the IO and western Pacific.

During the following spring, the wind difference increases. There are easterly differences over the western Pacific, indicating that the easterly wind anomaly in the western region becomes stronger, and the westerly wind in the eastern region becomes weaker in the case of IO warming. It is noted that the westerly wind also becomes weaker over the central Pacific even after normalization by the Niño-3.4 SST. This implies that IO warming can modulate not only the western Pacific wind, but also the central Pacific wind during the spring. These results support the notion that IO warming can induce additional easterly winds over the Pacific, which play a critical role in the ENSO transition.

In summary, during the El Niño developing phase, El Niño–related SSTs over the equatorial Pacific lead to IO warming through precipitation and wind responses, then IO warming can be intensified through local air-sea coupling. During the El Niño mature phase, IO warming begins to modulate the western Pacific precipitation and related easterly winds over the western Pacific, leading to the negative SST over the central to eastern Pacific via the oceanic process. The continuation of these processes into the following summer leads to a fast transition from El Niño to La Niña. In general, these dynamical processes simulated with climate models are quite consistent with those identified observationally (Kug and Kang 2006), though the overall patterns are shifted to the west in the climate models. Therefore, the MME results strongly support the hypothesized observed dynamical process for IO feedback suggested by previous studies (e.g., Kug and Kang 2006).

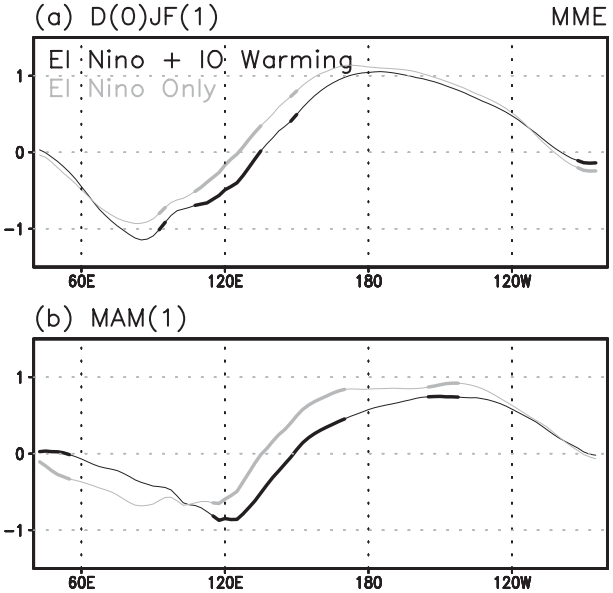

FIG. 7. The equatorial (5°S–5°N) 925-hPa MME zonal wind anomalies divided by the magnitude of Niño-3.4 SST from each composite in the IO warming case (red line) and the El Niño only case (blue line) during (a) D(0)JF(1) and MAM (1). Note that the thick line indicates that the difference between the two cases is significant at the 95% confidence level.

4. Model diversity in simulating IO feedback

In section 3, we showed that most of the climate models tend to simulate IO feedback reasonably, consistent with the observational findings. We also demonstrated the dynamical process of IO feedback on the ENSO transition based on the MME results. However, most of the models are likely to underestimate the strength of the IO feedback, and there is great diversity in simulating the strength of the IO feedback and the response of IO SST (Fig. 2). It would be useful to understand what causes this model diversity. In addition, from the analysis of model diversity, we can gain a clearer understanding of the dynamical process associated with the IO feedback and ENSO transition in climate models. Therefore, in this section, we assess the model diversity in IO feedback strength.

To examine the model diversity with regard to the strength of IO feedback, we formed the following two

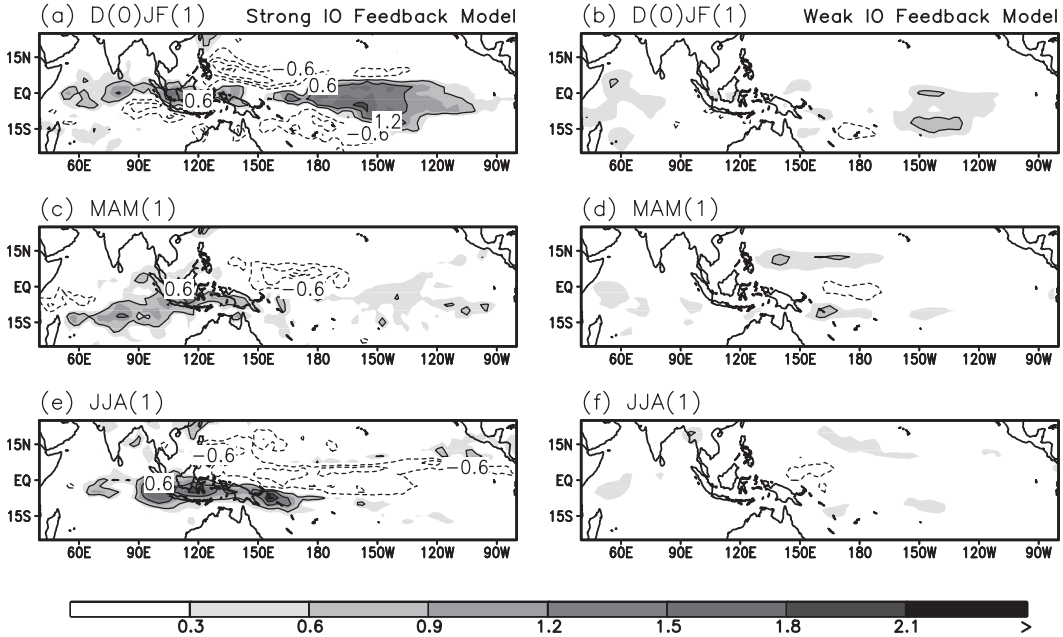

FIG. 8. The difference in precipitation in the IO warming case compared to that in the El Niño only case from the D(0)JF(1) to the JJA(1) season. (left)The precipitation difference in the strong IO feedback (SIOF) models is shown, and (right) the precipitation difference in the weak IO feedback (WIOF) models is shown.

groups from among the 18 models: strong IO feedback (SIOF) models and weak IO feedback (WIOF) models. From Fig. 2a, we selected four models, which contain CSIRO Mk3.0, CSIRO MK3.5, GFDL CM2.1, and INGV) ECHAM4 as SIOF models, and INM-CM3.0, CNRM-CM3, MRI CGCM2.3.2a, and CCCma_CGCM3.1 are selected as WIOF models. Figure 8 shows the precipitation difference between the IO warming and El Niño cases for each group. In general, the precipitation difference is relatively small in the WIOF models. Distinctive differences between the SIOF and WIOF models appear in the IO and WNP regions. In particular, the SIOF models show a strong positive precipitation difference over the equatorial IO during the D(0)JF(1) season.

Because the precipitation exhibits a dipole-like pattern over the IO in the IO warming case (Fig. 5c), the positive precipitation difference indicates an enhanced positive precipitation anomaly over the western IO and a weakened negative precipitation anomaly over the eastern IO. It is expected that the stronger positive precipitation anomaly over the western IO induces stronger WP easterlies, indicating strong IO feedback to the ENSO. On the other hand, it is quite interesting that the negative precipitation over the eastern IO is weakened in the SIOF in spite of the stronger El Niño magnitude. Because a stronger negative precipitation over the eastern IO can produce stronger low-level divergence, which induces anomalous westerlies over the WP, the transition to La Niña can be weakened if the eastern IO precipitation is too strong. Therefore, the weakened negative precipitation over the eastern IO is also linked to the strong IO feedback (i.e., transition from El Niño to La Niña during IO warming). In addition to the eastern IO, the positive precipitation difference appears over the Maritime Continent, which also indicates weakened negative precipitation. The weakened negative precipitation over the Maritime Continent is linked to the strong IO feedback in a similar way.

It is interesting that there is a negative precipitation difference over the southeastern IO during the D(0)JF(1) season (Fig. 8a). The negative precipitation difference indicates enhanced negative precipitation anomalies in that region (Fig. 5c). It is somewhat unclear how the enhanced negative precipitation is linked to the strong IO feedback. We suspect that the strong precipitation response in the southern region might be related to the southward shift of the eastern IO precipitation response. The southward shift of the precipitation response may be less effective in altering the equatorial WP wind, which is linked to stronger IO feedback.

Another distinctive difference appears over the WNP region. While the SIOF models show distinctive negative differences over the WNP during the D(0)JF(1) season, there is almost no signal in the WIOF models. Furthermore, during the following spring, the SIOF models show a negative difference, which favors

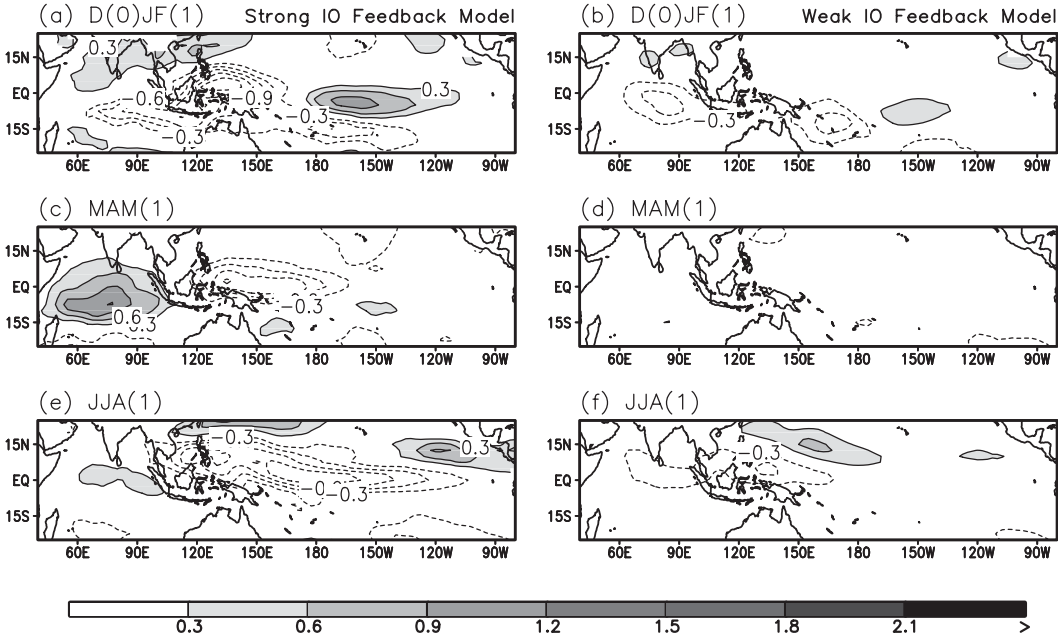

FIG. 9. As in Fig. 8, but zonal wind at 925-hPa anomalies.

anticyclonic circulation and equatorial easterlies. In contrast, the WIOF models show a positive precipitation difference in the MAM(1) season, which favors cyclonic circulation and equatorial westerlies. This plays a role in mitigating the ENSO transition. Therefore, these results indicate the precipitation responses to the IO warming over the IO and WNP differ between the SIOF and WIOF models, and they may be critical in determining the strength of the IO feedback.

Figure 9 shows the zonal wind difference between IO warming and El Niño only cases in the SIOF and WIOF groups. Consistent with the precipitation difference, the zonal wind is distinctively different in the SIOF models. It is quite evident that the WIOF models show a very weak difference over the whole Indo-Pacific regions. The easterly difference is dominant over the eastern IO and western Pacific during boreal winter in the SIOF models. In subsequent seasons, the most distinctive signals exist over the western Pacific, indicating that the western Pacific wind is the most critical component influencing IO feedback.

Figure 10 shows equatorial 925-hPa zonal wind anomalies for the two groups. To control for the dependence on El Niño magnitude, the zonal wind anomalies in each model are normalized by the magnitude of Niño-3.4 SST. With the aid of this normalization, the wind anomalies to the east of the international date line are found to be nearly the same between the IO warming and El Niño only cases. However, distinctive differences are still found over the IO and western Pacific in the SIOF models. For the El Niño only case, there are considerable easterly wind anomalies over the Indian Ocean though the IO SST anomalies are quite weak (blue line in Fig. 10a). It can be inferred that these easterly anomalies are induced by the western Pacific precipitation anomalies. For the IO warming case, the zonal wind anomalies tend to be shifted to the east. Therefore, the easterly anomalies are expanded to the western Pacific, and the westerly anomalies over the western Pacific are significantly weakened, which prefer to rapid termination of the positive eastern Pacific SST.

Conversely, in the WIOF models, the overall difference in wind anomalies is weak, consistent with Fig. 9. In addition, the magnitude of the wind anomalies over the Indian Ocean and western North Pacific is nearly zero in both the IO warming and El Niño only cases. This implies that the wind response to the SST forcing is weak in these models. The weak wind responses are linked to the weak precipitation responses as shown in Fig. 8.

As illustrated in Figs. 8 and 9, the spatial pattern of precipitation is critical for determining the strength of the IO feedback. To investigate what kind of spatial pattern is most related to the IO feedback strength, we generate a regression pattern based on the difference in precipitation between the IO warming and El Niño only cases with respect to the strength of the IO feedback from the 18 models. The strength of the IO feedback is defined as the difference in Niño-3.4 SST between the IO warming and El Niño only cases in the following the winter [D(1)JF(2)] season based on Fig. 2.

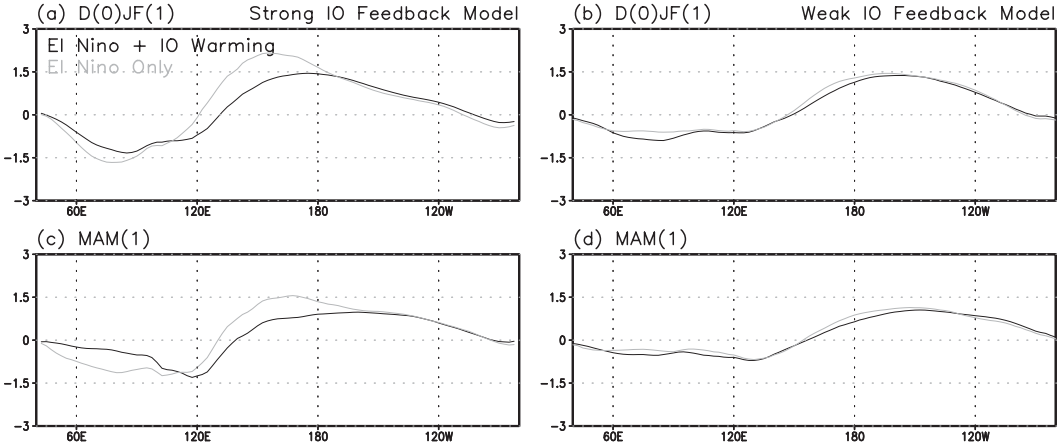

FIG. 10. The equatorial (5°S–5°N) zonal-wind anomalies at 925 hPa during the IO warming (black line) and El Niño only (gray line) cases in (left) the strong and (right) weak IO feedback models.

For brevity, the sign of the IO feedback strength is reversed so that a strong positive value indicates strong IO feedback. Based on the 18 precipitation difference maps and the IO feedback strength from each model, we assess the correlation between the precipitation difference and IO feedback strength and perform a regression analysis.

Figure 11 shows the regression pattern and the correlation between the precipitation difference and IO feedback strength. This regression pattern can be interpreted as the precipitation pattern that is most effective in inducing strong IO feedback associated with IO warming. To a large extent, the regression pattern is similar to the difference in SIOF shown in Fig. 8a. For the boreal winter season, we find four significant precipitation patterns: (i) positive precipitation from the western to central IO, (ii) negative precipitation over the southeastern IO, (iii) positive precipitation over the eastern IO to the Maritime Continent, and (iv) negative precipitation patterns in the off-equatorial WP. Most of these precipitation patterns play a role in enhancing equatorial WP easterlies as mentioned earlier. For example, a positive (negative) precipitation anomaly over the western to central IO (off-equatorial WP) leads to equatorial WP easterlies through the stationary Kelvin wave response (WNP anticyclone).

Comparing the spatial pattern shown in Fig. 5c with the regression pattern it becomes apparent that the regression pattern is somewhat similar to the precipitation anomalies associated with El Niño. That is, these precipitation patterns for strong IO feedback are generally related to the enhanced El Niño–related precipitation response, which implies that the strong precipitation responses tend to lead to strong IO feedback. However, it is noted that there is positive precipitation over the eastern IO to the Maritime Continent in Fig. 11a, contrary to the negative precipitation anomaly in Fig. 5c. This indicates that the weaker precipitation responses in those regions are linked to strong IO feedback because negative precipitation can induce the equatorial westerlies to the east of the precipitation.

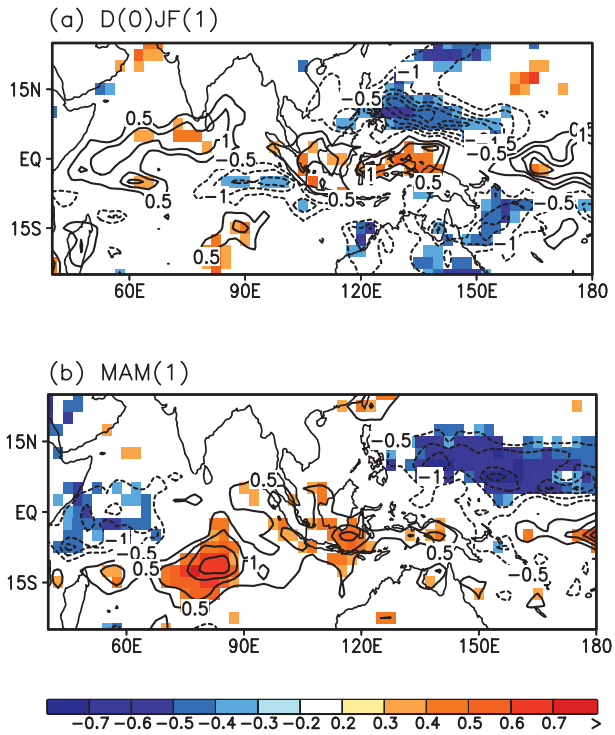

FIG. 11. The regression (contour) and correlation (shading) coefficients for the difference in precipitation between the two cases and IO feedback strength. The shaded correlation coefficients are significant at the 95% confidence level.

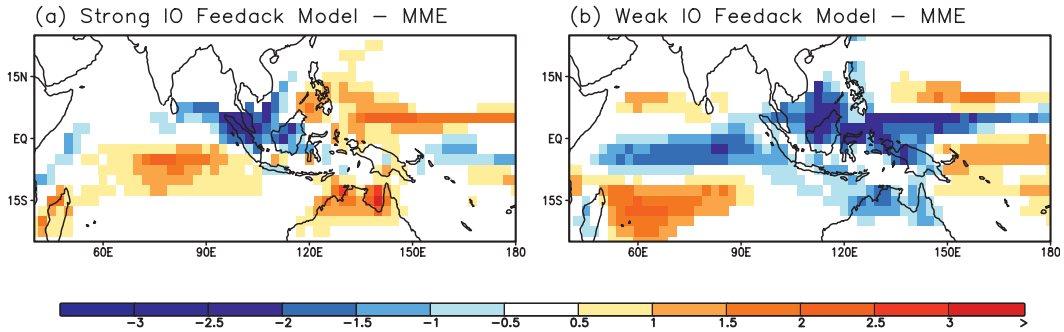

FIG. 12. The deviation in climatological DJF precipitation in the SIOF and WIOF models compared to the MME precipitation. The deviations that are significant at a 95% confidence level are shaded.

For the boreal spring season, the regression pattern is quite similar to the difference in SIOF as shown in Fig. 8c. In addition, compared to the precipitation composite associated with El Niño shown in Fig. 5c, the regression pattern indicates the presence of enhanced precipitation responses related to El Niño, especially over the eastern IO and WNP. It is therefore expected that the enhanced positive precipitation over the eastern IO and negative precipitation over the WNP will induce strong easterly anomalies over the equatorial Pacific, as mentioned earlier.

The precipitation responses in the climate models are related to the distribution of mean precipitation. In general, the precipitation response is strong where the mean precipitation is large. Figure 12 shows the deviation of the mean precipitation in the SIOF and WIOF models from the MME precipitation during the DJF season. It is clear that distinctive differences in the mean precipitation exist over the eastern IO, Maritime Continent and WNP regions, where the precipitation responses to El Niño and the IO SST are stronger. In particular, the SIOF models tend to simulate more climatological precipitation over the WNP and southeastern IO and less precipitation over the northeastern IO and Maritime Continent. It is quite interesting that the mean precipitation pattern in the SIOF models is similar to the regression pattern shown in Fig. 11a. The mean precipitation is relatively large where the precipitation response in the SIOF models is strong (i.e., over the WNP and southeastern IO), while the mean precipitation is small where the SIOF models simulate weak responses (i.e., over the northeastern IO and Maritime Continent). This trend indicates that the model diversity in terms of IO feedback can be partly explained by the diversity in mean precipitation. Furthermore, this implies that the mean climatology related to the precipitation over the warm pool region is critical in determining the IO feedback to the ENSO in climate models.

5. Summary and discussion

In this study, the IO feedback to the ENSO transition was investigated using CMIP3 models. Most climate models simulate a fast transition from El Niño to La Niña in the presence of IO warming. We found that the WP easterlies are critical for determining IO feedback to the El Niño transition. When IO warming induces equatorial easterlies over the western Pacific, it leads to a rapid termination of El Niño and consequently La Niña events tend to develop in the following year. These dynamic processes are quite consistent with the observations made in a previous study (Kug and Kang 2006).

Though most climate models simulate IO feedback reasonably, there is great diversity in the strength of the IO feedback. We found that the strength of the IO feedback is related to the precipitation response over the warm pool region (i.e., the western Pacific and eastern Indian Ocean). If the precipitation response over the WNP associated with El Niño and IO warming is strong, the models simulate strong IO feedback to the ENSO. In contrast, we determined that the IO feedback is stronger when the precipitation responses over the eastern IO to the Maritime Continent are weak. Interestingly, we found that the precipitation response is closely related to the spatial distribution of the mean precipitation over warm pool regions.

The fact that the climate models underestimate the IO feedback is notable, as is the considerable intermodel diversity in IO feedback strength. As we have emphasized, the WP easterlies are critical in determining IO feedback to the ENSO, which is closely related to the WNP anticyclone. It the climate models, this WNP-anticyclone-related equatorial easterly had little effect on the Pacific SST because the current climate models share a common problem in that they simulate El Niño–related anomalies westward-shifted compared to those in the observation. As shown in Fig. 13, the westward shift of the WNP anticyclone is also distinctive over the

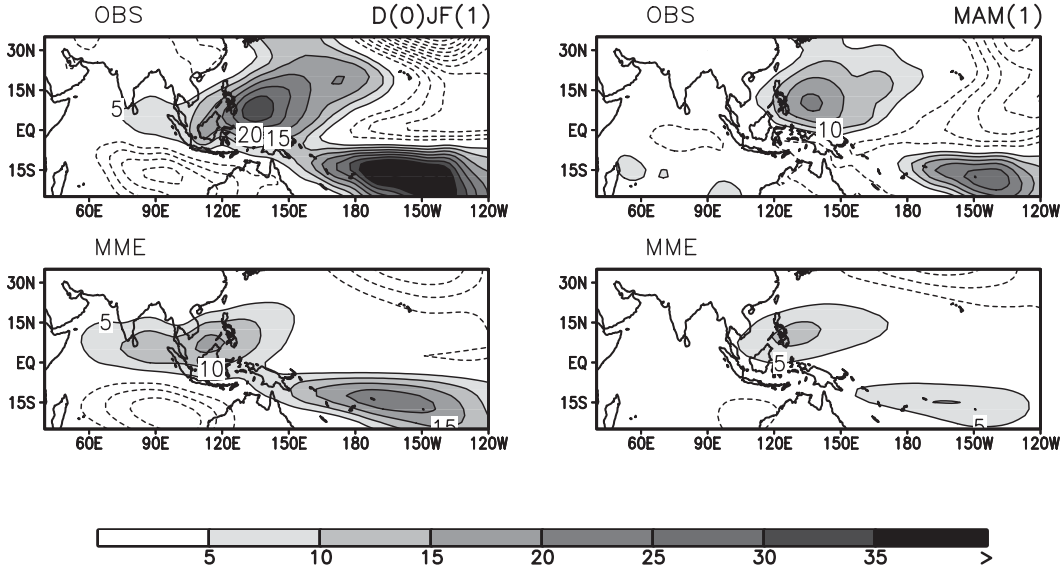

FIG. 13. The streamfunction anomalies at 925 hPa during the IO warming case in (top) observational model and (bottom) the MME during (left) the D(0)JF(1) and (right) MAM(1) seasons. The unit for the streamfunction anomalies is 10^5 m^2 s^{-1}.

IO and WNP regions. In particular, the center of the positive streamfunction (anticyclonic flow) over the WNP is located at 120°E, while the observational data indicates it is at 140°E during the D(0)JF(1) season. Corresponding to the shift, the equatorial easterlies are mainly located over the Maritime Continent (west of 120°E), and such anomalous easterlies over the continent cannot affect the dynamic oceanic field over the Pacific. Therefore, the westward shift of the easterlies means they have little impact on the region over the Pacific Ocean, resulting in weak IO feedback to the Pacific Ocean.

In this study, we focused primarily on the IO feedback for the warm phase. We found that IO feedback occurs during the cold phase of the ENSO (i.e., La Niña with IO cooling), but it is relatively weak both in observational (Kug and Kang 2006) and simulated models (Ohba et al. 2010; Ohba and Watanabe 2012). The weak IO feedback during the cold phase means that there is asymmetry in the strength of IO feedback to the ENSO and implies a relatively slow phase transition from La Niña to El Niño such that the duration of La Niña is expected to be longer than that of El Niño. Therefore, this asymmetric IO feedback may induce asymmetric ENSO characteristics, which are known to be derived from oceanic (An and Jin 2004; Su et al. 2010) and atmospheric nonlinearity (Kang and Kug 2002) over the Pacific. However, it is still unclear what causes this IO feedback strength asymmetry. This asymmetry could be important for ENSO prediction because it seems to determine the speed of the phase transition. Therefore, further study is required to fully understand the asymmetry in IO feedback strength and its implications.

Acknowledgments. This work is supported by the Korea Meteorological Administration Research and Development Program under Grant CATER 2012-3042.

REFERENCES

An, S.-I., and F.-F. Jin, 2004: Nonlinearity and asymmetry of ENSO. *J. Climate,* **17,** 2399–2412.

——, W. W. Hsieh, and F.-F. Jin, 2005: A nonlinear analysis of the ENSO cycle and its interdecadal changes. *J. Climate,* **18,** 3229–3239.

Annamalai, H., S.-P. Xie, J. P. McCreary, and R. Murtugudde, 2005: Impact of Indian Ocean sea surface temperature on developing El Niño. *J. Climate,* **18,** 302–319.

——, S. Kida, and J. Hafner, 2010: Potential impact of the tropical Indian Ocean Indonesian Seas on El Niño characteristics. *J. Climate,* **23,** 3933–3952.

Baquero-Bernal, A., M. Latif, and L. Stephanie, 2002: On dipole-like variability of sea surface temperature in the tropical Indian Ocean. *J. Climate,* **15,** 1358–1368.

Huang, B., and J. L. Kinter III, 2002: Interannual variability in the tropical Indian Ocean. *J. Geophys. Res.,* **107,** 3199, doi:10.1029/2001JC001278.

Izumo, T., and Coauthors, 2010: Influence of the state of the Indian Ocean Dipole on the following year's El Niño. *Nat. Geosci.,* **3,** 168–172.

Jin, F.-F., 1997a: An equatorial ocean recharge paradigm for ENSO. Part I: Conceptual model. *J. Atmos. Sci.,* **54,** 811–829.

——, 1997b: An equatorial ocean recharge paradigm for ENSO. Part II: A stripped-down coupled model. *J. Atmos. Sci.,* **54,** 830–847.

Kalnay, E., and Coauthors, 1996: The NCEP/NCAR 40-Year Reanalysis Project. *Bull. Amer. Meteor. Soc.,* **77,** 437–471.

Kang, I.-S., and J.-S. Kug, 2002: El Niño and La Niña sea surface temperature anomalies: Asymmetry characteristics associated with their wind stress anomalies. *J. Geophys. Res.,* **107,** 4372, doi:10.1029/2001JD000393.

Klein, S. A., B. J. Soden, and N. G. Lau, 1999: Remote sea surface temperature variation during ENSO: Evidence for a tropical atmosphere bridge. *J. Climate,* **12,** 917–932.

Krishnamurthy, V., and B. P. Kirtman, 2003: Variability of the Indian Ocean: Relation to monsoon and ENSO. *Quart. J. Roy. Meteor. Soc.,* **129,** 1623–1646.

Kug, J.-S., and I.-S. Kang, 2006: Interactive feedback between the Indian Ocean and ENSO. *J. Climate,* **19,** 1784–1801.

——, S.-I. An, F.-F. Jin, and I.-S. Kang, 2005: Preconditions for El Niño and La Niña onsets and their relation to the Indian Ocean. *Geophys. Res. Lett.,* **32,** L05706, doi:10.1029/2004GL021674.

——, B. P. Kirtman, and I.-S. Kang, 2006a: Interactive feedback between ENSO and the Indian Ocean in an interactive coupled model. *J. Climate,* **19,** 6371–6381.

——, T. Li, S.-I. An, I.-S. Kang, J.-J. Luo, S. Masson, and T. Yamagata, 2006b: Role of the ENSO-Indian ocean coupling on ENSO variability in a coupled GCM. *Geophys. Res. Lett.,* **33,** L09710, doi:10.1029/2005GL024916.

Lau, N.-C., and M. J. Nath, 2000: Impact of ENSO on the variability of the Asian–Australian monsoons as simulated in GCM experiments. *J. Climate,* **13,** 4287–4309.

——, and ——, 2003: Atmosphere–ocean variations in the Indo–Pacific sector during ENSO episodes. *J. Climate,* **16,** 3–20.

——, and ——, 2004: Simulation of tropical Indian Ocean SST variability with east–west asymmetry using a coupled atmosphere–ocean GCM. *J. Climate,* **17,** 245–265.

Li, T., Y. Zhang, E. Lu, and D. Wang, 2002: Relative role of dynamic and thermodynamic processes in the development of the Indian Ocean dipole: An OGCM diagnosis. *Geophys. Res. Lett.,* **29,** 2110, doi:10.1029/2002GL015789.

Li, Y., R. Y. Lu, and B. W. Dong, 2007: The ENSO–Asian monsoon interaction in a coupled ocean–atmosphere GCM. *J. Climate,* **20,** 5164–5177.

Luo, J.-J., R. Zhang, S. K. Behera, Y. Masumoto, F.-F. Jin, R. Lukas, and T. Yamagata, 2010: Interaction between El Niño and extreme Indian Ocean dipole. *J. Climate,* **23,** 726–742.

Ohba, M., and H. Ueda, 2007: An impact of SST anomalies in the Indian Ocean in acceleration of the El Niño to La Niña transition. *J. Meteor. Soc. Japan,* **85,** 335–348.

——, and ——, 2009: Role of nonlinear atmospheric response 608 to SST on the asymmetric transition process of ENSO. *J. Climate,* **22,** 177–192.

——, and M. Watanabe, 2012: Role of the Indo-Pacific interbasin coupling in predicting asymmetric ENSO transition and duration. *J. Climate,* **25,** 3321–3335.

——, D. Nohara, and H. Ueda, 2010: Simulation of asymmetric ENSO transition in WCRP CMIP3 multimodel experiments. *J. Climate,* **23,** 6051–6067.

Saji, N. H., and T. Yamagata, 2003: Structure of SST and surface win variability during Indian Ocean dipole mode events: COADS observation. *J. Climate,* **16,** 2735–2751.

——, B. N. Goswami, P. N. Vinayachandran, and T. Yamagata, 1999: A dipole mode in the tropical Indian Ocean. *Nature,* **401,** 360–363.

——, S. P. Xie, and T. Yamagata, 2006: Tropical Indian Ocean variability in the IPCC twentieth-century climate simulations. *J. Climate,* **19,** 4397–4417.

Smith, T. M., R. W. Reynolds, T. C. Peterson, and J. Lawrimore, 2008: Improvements to NOAA's historical merged land-ocean surface temperature analysis (1880–2006). *J. Climate,* **21,** 2283–2296.

Sooraj, K. P., J.-S. Kug, T. Li, and I.-S. Kang, 2009: Impact of El Niño onset timing on the Indian Ocean—Pacific coupling and subsequent El Niño evolution. *Theor. Appl. Climatol.,* **97,** 17–27, doi:10.1007/s00704-008-0067-8.

Su, J., R. Zhang, T. Li, X. Rong, J.-S. Kug, and C.-C. Hong, 2010: Causes of the El Niño and La Niña amplitude asymmetry in the equatorial eastern Pacific. *J. Climate,* **23,** 605–617.

Venzke, S., M. Latif, and A. Villwock, 2000: The coupled GCM ECHO-2. Part II: Indian Ocean response to ENSO. *J. Climate,* **13,** 1371–1383.

Wang, B., R. Wu, and X. Fu, 2000: Pacific-East Asia teleconnection: How does ENSO affect East Asian climate? *J. Climate,* **13,** 1517–1536.

Watanabe, M., 2008a: Two regimes of the equatorial warm pool. Part I: A simple tropical climate model. *J. Climate,* **21,** 3533–3544.

——, 2008b: Two regimes of the equatorial warm pool. Part II: Hybrid coupled GCM experiments. *J. Climate,* **21,** 3545–3560.

——, and F.-F. Jin, 2002: Role of Indian Ocean warming in the development of Philippine Sea anticyclone during ENSO. *Geophys. Res. Lett.,* **29,** 1478, doi:10.1029/2001GL014318.

——, and ——, 2003: A moist linear baroclinic model: Coupled dynamical–convective response to El Niño. *J. Climate,* **16,** 1121–1140.

Webster, P. J., A. M. Moore, J. P. Loschnigg, and R. R. Leben, 1999: Coupled ocean–atmosphere dynamics in the Indian Ocean during 1997-98. *Nature,* **401,** 356–360.

Wittenberg, A. T., A. Rosati, N. C. Lau, and J. J. Ploshay, 2006: GFDL's CM2 global coupled climate models. Part III: Tropical Pacific climate and ENSO. *J. Climate,* **19,** 698–722.

Wu, B., T. J. Zhou, and T. Li, 2009: Seasonally evolving dominant interannual variability modes of East Asian climate. *J. Climate,* **22,** 2992–3005.

——, T. Li, and T. J. Zhou, 2010: Relative contributions of the Indian Ocean and local SST anomalies to the maintenance of the western North Pacific anomalous anticyclone during the El Niño decaying summer. *J. Climate,* **23,** 2389–2403.

Wu, R., and B. Kirtman, 2004: Understanding the impacts of the Indian Ocean on ENSO variability in a coupled GCM. *J. Climate,* **17,** 4019–4031.

Xie, S.-P., H. Annamalai, F. A. Schott, and J. P. McCreary Jr., 2002: Structure and mechanisms of South Indian Ocean climate variability. *J. Climate,* **15,** 864–878.

——, K. Hu, J. Hafner, H. Tokinaga, Y. Du, G. Huang, and T. Sampe, 2009: Indian Ocean capacitor effect on Indo-western Pacific climate during the summer following El Niño. *J. Climate,* **22,** 730–747.

Yamanaka, G., T. Yasuda, Y. Fujii, and S. Matsumoto, 2009: Rapid termination of the 2006 El Niño and its relation to the Indian Ocean. *Geophys. Res. Lett.,* **36,** L07702, doi:10.1029/2009GL037298.

Yang, J. L., Q. Y. Liu, S.-P. Xie, Z. Y. Liu, and L. X. Wu, 2007: Impact of the Indian Ocean SST basin mode on the Asian summer monsoon. *Geophys. Res. Lett.,* **34,** L02708, doi:10.1029/2006GL028571.

Yu, J.-Y., 2005: Enhancement of ENSO's persistence barrier by biennial variability in a coupled atmosphere-ocean general circulation model. *Geophys. Res. Lett.,* **32,** L13707, doi:10.1029/2005GL023406.

——, and K. M. Lau, 2005: Contrasting Indian Ocean SST variability with and without ENSO influence: A coupled atmosphere–ocean GCM study. *Meteor. Atmos. Phys.,* **90,** 179–191, doi:10.1007/s00703-004-0094-7.

——, C. R. Mechoso, J. C. McWilliams, and A. Arakawa, 2002: Impacts of the Indian Ocean on the ENSO cycle. *Geophys. Res. Lett.,* **29,** 1204, doi:10.1029/2001GL014098.